# Microstructure formation in electrodeposited Co-Cu/Cu multilayers with GMR effect: influence of current density during the magnetic layer deposition

D. Rafaja[a], C. Schimpf[a], T. Schucknecht[a], V. Klemm[a], L. Péter[b], I. Bakonyi[b]

[a]) Institute of Materials Science, TU Bergakademie Freiberg, Gustav-Zeuner-Str. 5, D-09599 Freiberg, Germany

[b]) Research Institute for Solid State Physics and Optics, Hungarian Academy of Sciences. H-1525 Budapest, P.O. Box 49, Hungary

**Abstract**

The influence of the current density applied during the deposition of the magnetic layers on the microstructure formation in electrodeposited Co-Cu/Cu multilayers and on their giant magnetoresistance (GMR) was investigated using a combination of magnetoresistance measurements, wide-angle and small-angle X-ray scattering, high-resolution transmission electron microscopy, atomic force microscopy and chemical analysis. The magneto-resistance measurements revealed that a reduction of the current density stimulates a transition from the formation of the magnetic layers with predominantly ferromagnetic character to the formation of superparamagnetic regions. As based on electrochemical considerations, it was supposed that such a change in the magnetic properties can be caused by an increased amount of Cu codeposited with Co at low current densities. It turned out from the structural studies that a pronounced segregation of Co and Cu occurs at low current densities. In accordance with their very low mutual solubility at room temperature, no atomic scale intermixing of Co and Cu could be detected. The segregation of Cu and Co was related to the fragmentation of the magnetic layers, to the enhancement of the local lattice strains, to the increase of the interface corrugations, to the partial loss of the multilayer periodicity and finally to the formation of Co precipitates in the Cu matrix.

Keywords: electrodeposition, multilayers, giant magnetoresistance, microstructure, X-ray scattering, transmission electron microscopy

## *1. Introduction*

Multilayers with the giant magnetoresistance (GMR) effect [1, 2] became in the last two decades a key element in the development of the reading heads of magnetic storage devices. Although such magnetoresistive sensors are currently produced mainly by using physical methods, the electrodeposition is still considered as a potential cost-effective alternative [3]. A recent review on this topic [4] lists almost 150 papers that were published on electrodeposited (ED) multilayers with GMR. Despite the large number of papers and the occasional correlations found between the parameters of the electrochemical deposition process and the GMR properties measured, very little is known about the microstructure of these multilayers and about the correlation between the microstructure and the parameters of the electrochemical deposition process. A particular problem is still a large interface roughness of ED multilayers and the formation of precipitates as already reported in References [5 – 7].

In order to protect the ED GMR multilayers against oxidation during the deposition, the so-called single-bath electrodeposition method [3, 4] was developed. The electrolyte contains both components to be deposited; the salt of the less noble ferromagnetic (FM) element (Co) is applied in a fairly high concentration, while the salt of the more noble non-magnetic (NM) metal (Cu) is used as a minor bath component. The Co and Cu layers are deposited by using high-current and low-current pulses, respectively, or alternatively by using high-potential and low-potential pulses. In order to achieve a significant GMR effect, the Cu layers should be free of Co that can be easily ensured by an appropriate choice of the Cu deposition current or potential [4, 8, 9]. Vice versa, the single-bath deposition of Co layers that are free of Cu is nearly impossible. The Co layers deposited during the high-current (or high-potential) pulse always contain some amount of Cu. The concentration of Cu in the Co layers depends strongly on the deposition conditions.

Furthermore, the competing electrochemical processes (deposition of Cu, deposition and dissolution of Co) can affect the thickness of individual layers if the layer thicknesses are controlled through Faraday's law on a charge-balance basis. The layer thickness estimated from Faraday's law agrees best with the real layer thickness when neither the exchange reaction [10] nor the dissolution of the previously deposited magnetic layer [8] can take place during the deposition of the NM layers. For electrodeposited FM/NM multilayers, it was concluded in Refs. 8 and 9 that these requirements can conveniently be achieved by using a combination of the galvanostatic and potentiostatic (G/P) deposition modes. The FM layers are deposited in the G mode and the NM layers in the P mode. The potential applied for deposition of the NM layers has to be optimized, e.g., with the aid of the analysis of the current transients recorded during the NM layer deposition pulse as described in Ref. 9.

In a previous work by Liu et al. [11], a series of ED Co-Cu/Cu multilayers prepared in the G/P mode with an optimized Cu deposition potential was investigated. The amount of Cu atoms incorporated into the magnetic layers was modified by changing the concentration of the $Cu^{2+}$ ions in the bath; all other parameters of the deposition process were kept constant. The decomposition of the dependence of the magnetoresistance (MR) on the magnetic field according to Ref. [12] revealed two contributions to the GMR effect, i.e., the regular FM component and a superparamagnetic (SPM) component, and helped in their quantification. It was found that the SPM component becomes stronger with increasing concentration of $Cu^{2+}$ ions in the bath and thus with increasing Cu content in the Co layers [11]. The SPM component was attributed to the formation of SPM regions in the magnetic multilayers. Whilst the SPM contribution to the total GMR increased with increasing Cu content in the Co layers, a reduction of the size of the SPM regions was concluded.

Based on the results of the MR measurements [11], it was assumed that the SPM regions arise via fragmentation of the magnetic layers. However, this statement was not proven directly by a detailed structural study, but it was mainly justified by a negligible miscibility of Cu and Co at room temperature. The present work describes the microstructure formation in the ED Co-Cu/Cu multilayers with different amount of Cu in the FM layers and attempts to explain the interplay between the microstructure and the magnetoresistance in more detail. The Cu concentration in the Co layers was modified through the current density $j_{mag}$, which was applied during the deposition of the magnetic layers.

### *2. Experimental details*

Three Co-Cu/Cu multilayers with the same number of bilayers and with the same desired thickness of the respective layer, $[Co(3.3\ nm)/Cu(4.0\ nm)]^{91}$, were electrochemically deposited in the mixed G/P mode [8]. The Cu layers were deposited at a constant electrode potential of -0.6 V (vs. SCE) that was optimized to avoid both the dissolution of the preceding Co layer and the Co codeposition during the Cu deposition pulse [4,9]. This guarantees a good agreement between the real layer thickness and the layer thickness determined from Faraday's law. The magnetic layers were deposited in the galvanostatic mode, which allows a convenient control of the layer thickness according to Faraday's law and helps to eliminate the uncertainty of the control parameters due to the ohmic drop effect. For the deposition of the magnetic layers, the following current densities were applied to modify the amount of Cu codeposited with Co: $j_{mag}$ = 84 mA·cm$^{-2}$ (sample A), $j_{mag}$ = 20.7 mA·cm$^{-2}$ (sample B) and $j_{mag}$ = 9.6 mA·cm$^{-2}$ (sample C).

The electrodeposition was carried out in a columnar cell, in which the sample was mounted horizontally at the bottom [8, 13]. The electrolyte contained sulphate salts of the metallic species (0.8 mol l$^{-1}$ $CoSO_4$ and 0.015 mol l$^{-1}$ $CuSO_4$) and additions of 0.2 mol l$^{-1}$ boric

acid ($H_3BO_3$) and 0.2 mol $l^{-1}$ ammonium sulphate ($(NH_4)_2SO_4$). The whole deposition process was computer-controlled; a combined potentiostat/galvanostat (EF453 from Electroflex, Hungary) was used as a source of the current for deposition. The Co-Cu/Cu multilayers were deposited on polished (100) oriented Si wafers, which were first covered with a buffer system consisting of a 5 nm thick Cr and a 20 nm thick Cu layer in a vacuum evaporation process. Atomic force microscopy (AFM) revealed the surface roughness of the evaporated Cu seed layer of about 1 nm [14]. Each ED multilayer stack started with a Co layer and ended with a Cu layer to protect the multilayer from later oxidation. The deposition parameters are summarized in Table 1 together with the mean thickness of the individual layers as determined from Faraday's law.

The chemical composition of the ED Co-Cu/Cu multilayers was inspected using the energy-dispersive analysis of characteristic X-rays (EDX) in an analytical transmission electron microscope (TEM) and verified by EDX analysis performed in a scanning electron microscope (SEM). The measurements in TEM were done on cross-sectional specimens, the SEM measurements on the surface of the as-deposited multilayers. This combination of the complementary techniques was applied to avoid the influence of systematic errors of both methods as far as possible. Room-temperature magnetoresistance was measured on 1 to 2 mm wide strips of the ED multilayers using the four-point-in-line method in the field-in-plane/current-in-plane geometry. The magnetic field was varied in the range of ± 800 mT. Both the longitudinal (current parallel to magnetic field, LMR) and the transversal (current perpendicular to magnetic field, TMR) components of the magnetoresistance were measured.

The microstructure of the multilayers was investigated by using TEM, wide-angle and small-angle X-ray scattering (WAXS and SAXS) and AFM. TEM was done on JEM 2010 FEF equipped with a field-emission gun that was operated at 200 keV. The cross-sectional specimens for TEM were prepared from two pieces of the respective multilayers. The counterparts were mounted face to face in a special sample holder that allowed their cutting, mechanical pre-thinning (dimpling) and etching by the Ar ion beam. The final step in the sample preparation was a plasma cleaning procedure. Symmetrical WAXS experiments were carried out on a Seifert/FPM RD7 diffractometer that was equipped with a sealed X-ray tube with copper anode ($\lambda$ = 0.15418 nm) and a curved graphite monochromator located in front of a scintillation detector. Asymmetrical WAXS and SAXS measurements were performed on a D8 diffractometer (Bruker AXS) that was equipped with a sealed X-ray tube with copper anode and a parabolic Goebel mirror in the primary beam. The latter produced a sufficiently parallel beam with the divergence of approx. 150'', which allowed the sample to be tilted without defocusing of the scattered beam. The asymmetrical WAXS patterns were carried out in the glancing-angle X-ray diffraction (GAXRD) geometry, with a constant and small

angle of incidence of the primary beam on the sample surface (3°). The SAXS patterns were measured in form of the sample scans (rocking curves) at fixed detector angles. For AFM, a Topometrix Discoverer TMX-2010 operating in contact mode was employed. Square areas with the size of 10 × 10 μm² were scanned for each sample; the effect of the inclined surface was corrected through a diagonal line-scan prior to data acquisition.

## *3. Results*

### *3.1 Magnetoresistance*

Magnetoresistance curves shown in Fig. 1 were determined from the measured resistivity R(H) according to

$$MR = \frac{R(H) - R_{\max}}{R_{\max}}, \qquad (1)$$

where $R_{max}$ is the maximum resistivity observed in the vicinity of zero magnetic field. The magnetoresistance measurements revealed significant changes in the magnetotransport with the current density $j_{mag}$. For sample A deposited at the highest current density ($j_{mag}$ = 84 mA/cm²), a GMR effect with negative LMR and TMR components was observed. In Fig. 1a, rapid saturation of the magnetoresistance in both longitudinal and transversal configurations can be seen above about 200 mT that is typical for FM/NM multilayers. The low SPM contribution to the total MR (Fig. 1b) indicates a high degree of continuity of the magnetic layers in sample A that are well separated from each other by continuous non-magnetic Cu layers. A similar behavior was observed for sample B, for which the magnetic layers were deposited at the medium current density ($j_{mag}$ = 20.7 mA/cm²). Nevertheless, the reduction of $j_{mag}$ from 84 mA/cm² to 20.7 mA/cm² led to a slight enhancement of MR at higher magnetic fields (Fig. 1a) that was induced by augmentation of both the FM and SPM components (Fig. 1b). The difference between LMR and TMR (solid and open symbols in Fig. 1a) measured at high magnetic fields is a measure of the anisotropic magnetoresistance (AMR) [15], which arises due to the bulk behavior of the FM layers. The AMR magnitude is approximately the same for samples A and B, about 0.4 %. The splitting of the MR curves in the vicinity of the zero field is caused by the coercivity of the remagnetization process. MR has its maximum at 10.8 mT and 15.1 mT for samples A and B, respectively (Fig. 1c). These values of the magnetic field agree well with the values (approx. 8 mT) reported in [16] for ED Co/Cu multilayers with similar layer thicknesses, $H(R_{max}) \approx 8$ mT.

Rather different behavior was observed for sample C deposited at $j_{mag}$ = 9.6 mA/cm², in which the SPM component dominated the GMR effect and only a very low FM contribution was observed. Moreover, the SPM component increased significantly even at magnetic fields of ± 800 mT (Fig. 1b). The AMR contribution to the observed magnetoresistance practically

vanished; the LMR and TMR were almost the same. This means that sample C does not contain extensive ferromagnetic regions. Furthermore, the MR curves of sample C do not exhibit hysteresis; the MR peak lies practically at zero magnetic field that confirms the assumption of the dominating SPM contribution to the total magnetoresistance.

*3.2 Multilayer periodicity and interface corrugations*

A progressive decay of the superlattice satellites in the WAXS patterns (Fig. 2) indicated an overall decrease of the multilayer quality with decreasing $j_{mag}$. In periodic multilayers, the reduction of the intensity of the satellites is generally attributed to a large variation of the bilayer thickness [17] that can be caused by a loss of the multilayer periodicity and/or by an enlargement of the uncorrelated interface corrugations. Accordingly, a good multilayer periodicity and a small uncorrelated interface roughness was supposed for sample A deposited at $j_{mag}$ = 84 mA/cm². Both features were confirmed by the TEM micrograph (Fig. 3) that was taken in a strong overfocus [18] in order to improve the intrinsically low scattering contrast of Co and Cu for electrons. Furthermore, TEM revealed huge but highly correlated interface corrugations. As the highly correlated interface corrugations do not lead to a considerable variation of the bilayer thickness, they usually do not destroy the superlattice satellites in the WAXS patterns.

Significant decrease of the intensity of the superlattice satellites and their broadening was observed in the WAXS pattern of sample B ($j_{mag}$ = 20.7 mA/cm²). Both phenomena suggest that the bilayer thickness varies in a certain range. According to Eq. (2) taken from Ref. [17], the bilayer thickness ($\Lambda$) affects directly the positions of the superlattice satellites ($\theta_n$):

$$\frac{2\sin\theta_n}{\lambda} = \frac{1}{\langle d \rangle} \pm \frac{n}{\Lambda} \tag{2}$$

In Eq. (2), $\lambda$ means the wavelength of the X-rays, *n* the satellite order and $\langle d \rangle$ the mean interplanar spacing of the multilayer system:

$$\langle d \rangle = \frac{N_{Cu} d_{Cu} + N_{Co-Cu} d_{Co-Cu}}{N_{Cu} + N_{Co-Cu}} = \frac{\Lambda}{N_{Cu} + N_{Co-Cu}} \tag{3}$$

In Eq. (3), $N_X$ means the average number of atoms in the layers with the interplanar spacing $d_X$. Consequently, a variation of the bilayer thickness in a multilayer stack leads to a superposition of satellite maxima with different distances from the central peak, which causes the broadening of the superlattice satellites in WAXS pattern and the reduction of their intensity.

TEM micrograph (Fig. 4) showed highly correlated interface corrugations also in sample B. However in contrast to sample A, where the individual layers were corrugated but continuous over large lateral distances, the multilayer in sample B apparently grows in form

of columnar grains. The bits of the multilayer stack seem to be terminated by the grain boundaries. As the micrograph was taken in the focus, the diffraction contrast in Fig. 4 is much stronger than the scattering contrast between Cu and Co. The possible sources of the diffraction contrast are local strain fields and different crystallographic orientations of the dark and bright regions.

The fitting of WAXS patterns according to the approach introduced by Fullerton *et al* [17] revealed the mean bilayer thickness, the mean thicknesses of FM and NM layers and their variations, and the interplanar spacing of the respective layer. The results of the fitting are shown by solid lines in Fig. 2 for samples A and B. The refined values of the above microstructure parameters are summarized in Table 2. As shown in Table 1, the bilayer thickness determined using Faraday's law was larger in sample B than in sample A. The bilayer thicknesses calculated from the WAXS patterns (Table 2) were opposite, as it corresponds to larger distances between the superlattice satellites in the WAXS pattern of sample B as compared with sample A (Fig. 2). This particular result is illustrated in Table 3 on the ratio of the bilayer thicknesses and on the ratio of the individual layer thicknesses, which were obtained from Faraday's law and from fitting of the WAXS patterns.

The relative decrease of the bilayer thickness in sample B as compared to sample A (Table 3), large fluctuations of the bilayer thickness (Fig. 2), formation of columnar grains (Fig. 4) and presence of the bent layers pinned at the grain boundaries (Fig. 4) strongly supports the hypothesis that Cu codeposited in sample B with Co segregates predominantly near the boundaries of the columnar grains. Consequently, the regions adjacent to the grain boundaries contain more Cu and less Co than the parts of the multilayer structure located in the centre of the columnar grains. This lateral segregation of Cu and Co codeposited during the deposition of the magnetic layers can explain both the large fluctuation of the bilayer thickness and the reduction of the bilayer thickness revealed by WAXS. As Cu segregated at the grain boundaries is not a part of the periodic motif, it contributes neither to the bilayer thickness nor to the thickness of the individual Cu layers.

A further reduction of the current density to $j_{mag}$ = 9.6 mA/cm² (sample C) led to a disappearance of the superlattice satellites in the WAXS pattern (Fig. 2). In [19], this phenomenon was explained by formation of precipitates of one atomic species in the matrix of the other atomic species instead of a periodic multilayer structure. In sample C, the disappearance of the periodic multilayer structure was confirmed by TEM (Fig. 5). The TEM/EDX analysis of the chemical composition of the ED Co-Cu/Cu multilayers helped us to understand the enormous degradation of the multilayer structure in sample C, which was followed by the rise of the SPM component and by the decay of the FM contribution to the total magnetoresistance. Whereas the Co and Cu contents in samples A and B did not deviate from their expected values within the expected experimental accuracy of the

TEM/EDX analysis, sample C contained much more copper than cobalt. This result of the TEM/EDX analysis was confirmed with the EDX analysis in SEM. Based on this result of the EDX analyses we can conclude that the matrix consists of Cu, whereas the precipitates contain Co as the main components. The difference in the overall chemical composition of the ED Co-Cu/Cu multilayers under study is clearly visible from the different intensities of the spectral lines CoK$\alpha$/CoK$\beta$ and CuK$\alpha$/CuK$\beta$ in Fig. 6.

*3.3 Surface roughness and morphology*

The interface corrugations discussed in the previous section grew through the whole multilayer up to the sample surface. This authorizes the surface roughness to be employed as an additional indicator of the interface corrugations. For the measurement of the surface roughness, SAXS and AFM were applied as two complementary methods because of their different sensitivity on different length scales. Whereas SAXS probes the surface roughness up to some tens of nanometers, AFM recognizes substantially larger objects.

The SAXS patterns were taken in form of the rocking curves (Fig. 7). Due to a low X-ray scattering contrast between Cu and Co, the main features visible in the rocking curves are the specular reflectivity (at $\omega = 0$) [20], the Yoneda wings [21] and the diffuse scattering around the specular reflectivity maximum [22 – 24]. With respect to the surface roughness, the intensity of the Yoneda wings is the most sensitive parameter; it decreases rapidly with increasing amplitude of the surface corrugations [22]. Accordingly, sample B has the highest surface roughness among the samples under study. The diffuse scattering concentrated at the specular reflectivity maximum arises mainly from the X-ray scattering on laterally non-continuous interfaces [19]. Consequently, the different extent of the diffuse scattering in the rocking curves shown in Fig. 7 can be interpreted as a continuous increase of the discontinuity of the magnetic layers with decreasing $j_{mag}$. The increase of the diffuse scattering in sample B (as compared to sample A) can be assigned to the formation of columnar grains and to the segregation of Cu at the grain boundaries as discussed in Section 3.2, a further intensification of the concentrated diffuse scattering in sample C to the formation of Co precipitates in Cu matrix.

The maximum surface roughness in sample B concluded from the disappearance of the Yoneda wings was complemented by results of AFM (Fig. 8). The rms surface roughness increased from (10.5 ± 2.1) nm in sample A to (21.8 ± 1.2) nm in sample B and decreased to (19.5 ± 2.1) nm in sample C. A possible reason for the non-monotonous dependence of the surface roughness on $j_{mag}$ that was observed both by SAXS and AFM is the laterally inhomogeneous deposition of Co and Cu during the magnetic layer deposition. As discussed in Section 3.2, in sample B having the maximum correlated interface roughness, Cu codeposited with Co segregates predominantly near the boundaries of the columnar grains

and causes large fluctuation of the bilayer thickness. Consequently, the interface roughness rises towards the surface of the multilayer and is responsible for the maximum of the surface roughness in sample B. The surface roughness in sample C is reduced to some extent because Co precipitates are overgrown by Cu matrix.

*3.4 Lattice strain and lattice defects in the multilayers*

Another reason for the formation of interfaces with strongly correlated corrugations is the presence of local strain fields in samples A and B. In Section 3.2, the local strain fields were regarded as a possible source of the diffraction contrast in the TEM micrograph from Fig. 4. In this Section, the existence of the local strain fields is proven via analysis of the interplanar spacings of Co and Cu that were obtained from the symmetrical WAXS measurements (Table 2). As discussed in [7], just one Cu modification but two Co modifications have to be considered in ED Co-Cu/Cu multilayers: face-centered cubic (fcc) Cu, fcc Co and hexagonal close packed (hcp) Co. Although hcp Co is the stable phase at room temperature, fcc Co can be stabilized at Co/Cu interfaces [7]. The intrinsic interplanar spacings next to the measured interplanar spacings from Table 2 are $d^0_{111}$ (fcc Cu) = 0.20871 nm, $d^0_{111}$ (fcc Co) = 0.20465 nm and $d^0_{002}$ (hcp Co) = 0.20303 nm [25]. Together with the measured interplanar spacings from Table 2, the above intrinsic interplanar spacings ($d^0_{hkl}$) were employed to calculate the lattice strains in Cu and Co layers given in Table 4 according to:

$$\varepsilon_{\perp}(X) = \frac{d_{meas}(X) - d^0_{hkl}(X)}{d^0_{hkl}(X)} \tag{4}$$

As these WAXS experiments were performed in the symmetrical mode, the measured interplanar spacing and the lattice strain calculated according to Eq. (4) refer to the direction perpendicular to the sample surface. In sample A, Cu layers were under a small tensile stress. The interplanar spacing measured in Co layers lay between $d^0_{111}$ (fcc Co) and $d^0_{002}$ (hcp Co). Therefore, Co layers were apparently under a tensile stress, if the measured interplanar spacing was related to $d^0_{111}$ (fcc Co), and under a compressive stress, if the measured interplanar spacing was related to $d^0_{002}$ (hcp Co). For an "average" interplanar spacing of fcc and hcp Co ($\langle d \rangle$ = 0.20384 nm), the deformation of the Co lattice measured in the direction perpendicular to the sample surface was positive, which corresponds to a compressive stress in Co layers. The magnitude of this lattice deformation in Co was very close to the lattice deformation observed in Cu layers. This means that a stress-equilibrium state at the Cu/Co interfaces can be reached if the interplanar spacing in Co can very between its extreme values $d^0_{111}$ (fcc Co) and $d^0_{002}$ (hcp Co). In [7], it was shown that such a

variation of the interplanar spacing in Co can be achieved through stacking faults or microtwins grown perpendicular to the growth direction of the multilayer stack.

In sample B, the lattice deformation $\varepsilon_\perp$ (fcc-Cu) was much higher than in sample A. As $d_{meas}$(Co) was even higher than $d^0_{111}$ (fcc Co), the lattice stress was compressive independent of the choice of the reference intrinsic interplanar spacing, i.e. $d^0_{111}$ (fcc Co) or $d^0_{002}$ (hcp Co). The relative lattice deformation in Co layers calculated using $\langle d \rangle$ arrived at nearly the same magnitude like for Cu layers, which indicates the stress-equilibrium state as discussed for sample A. Microtwins, which accompany the change of the interplanar spacing between $d^0_{111}$ (fcc Co) and $d^0_{002}$ (hcp Co), were found by TEM in sample B as well (Fig. 9). Furthermore, TEM helped to visualize the strain fields, which were predicted in sample B by WAXS (Table 4). According to Fig. 10, the strain fields follow the curvature of interfaces, which was regarded above as the main component of the interface corrugation.

In sample C, the interplanar spacing of neither Co nor Cu could be calculated from WAXS pattern because of missing superlattice satellites (Fig. 2). WAXS recognized predominantly the diffraction maximum from the Cu matrix [19]; the contribution of the Co precipitates to the WAXS signal was negligible. Still, a shift of the diffraction maximum to higher diffraction angles was observed, which corresponds to a decrease of the interplanar spacing $d_{111}$(Cu) with regard to its intrinsic value and consequently to a tensile stress in Cu matrix. The corresponding lattice deformation calculated from Eq. (4) for $d_{111}$(Cu) = (0.20805 ± 0.00003) nm and $d^0_{111}$(Cu) = 0.20871 nm was $\varepsilon_\perp$ (fcc-Cu) = -(3.2 ± 0.2) × $10^{-3}$. Additional information on lattice deformation was obtained from the $\sin^2\psi$ method [26] applied to GAXRD data. For fcc Cu, the $\sin^2\psi$ method revealed the lattice parameter both in the plane of the sample and in the sample surface perpendicular direction. The in-plane lattice parameter and the corresponding interplanar spacing were $a_\parallel$ = (0.36164 ± 0.00005) nm and $d_\parallel$ = (0.20879 ± 0.00005) nm, respectively; the analogous quantities obtained for the sample surface perpendicular direction were $a_\perp$ = (0.36041 ± 0.00005) nm and $d_\perp$ = (0.20808 ± 0.00005) nm.

Within the experimental accuracy, $d_\parallel$ is nearly equal to $d^0_{111}$(Cu) but $d_\perp$ is smaller, which confirms the tensile stress that was concluded already from the symmetrical WAXS measurement. Obviously, the interplanar spacing $d_\perp$ measured by GAXRD must agree with the interplanar spacing measured by symmetrical WAXS. The difference between these interplanar spacings is a measure of the experimental error. As noted above, the positive difference between $d_\parallel$ and $d_\perp$ indicates a tensile stress in Cu in sample C, but the lattice strain estimated from this difference according to [27], $\varepsilon = \left(d_\perp - d_\parallel\right) / \left(2d^0_{111}\right) = -1.7 \times 10^{-3}$, was smaller than $\varepsilon_\perp$ (fcc-Cu) = -(3.2 ± 0.2) × $10^{-3}$ that was obtained from the symmetrical

WAXS. The reason for this discrepancy was an “improper” reference interplanar spacing $d_{111}^{0}$(Cu). The “true” reference interplanar spacing $d_{111}^{0}$(Cu) calculated using the approach from [26] for the Poisson ratio of 0.35 and for $d_{||}$ and $d_{\perp}$ given above was equal to 0.2085(1) nm.

The combination of symmetrical WAXS and asymmetrical GAXRD measurements carried out on sample C has shown that the tensile stress in Cu is, to a certain extent, caused by the electrochemical deposition process and not exclusively by the interaction between Co and Cu at their interfaces. As discussed above and summarized in Table 4, tensile stress in Cu was observed in all ED Co-Cu/Cu multilayers under study.

**4. Discussion**

As based on electrochemical considerations, it was assumed that a decrease of current density applied during the deposition of magnetic layers ($j_{mag}$) in ED Co-Cu/Cu multilayers enhances the amount of Cu codeposited with Co. Therefore, the central task of this work was to clarify, where the codeposited Cu atoms are located in the multilayer structure. Because of a negligible miscibility of Co and Cu below 422°C [28], it was supposed that Cu atoms are not incorporated in the crystal structure of cobalt in a significant fraction, but segregate and build self-contained clusters. However, a direct experimental verification of this hypothesis was awkward. Local chemical analysis, even by EDX in scanning TEM, was practically impossible because of the small individual layer thickness, high interface corrugations and a lot of instrumental factors affecting the accuracy of the chemical analysis in TEM. Sole analysis of the interplanar spacings using WAXS could not provide clear results as well, because the effect of the chemical composition on the interplanar spacing is overlaid by the change of the interplanar spacing through lattice deformation.

Nevertheless, detailed microstructure analysis comprising the investigation of the multilayer periodicity, interface corrugations, formation of columnar grains and lattice strains for different current densities $j_{mag}$ has shown that the codeposition of Cu with Co during the magnetic layer deposition does not lead necessarily to an intermixing of the codeposited species at the atomic level. Instead, a selective deposition of the elements was concluded from the observed formation of pinholes filled with Cu, which substantially contributed to the discontinuity of the magnetic layers. At a high degree of the codeposition of Cu with Co, the deposition of the elements with a large lateral selectivity led to the growth of Co precipitates in the Cu matrix.

Lateral segregation of Co and Cu during pulse plating was already discussed in [29]. One of the phenomena, which facilitate the lateral segregation of the deposited species, is their surface diffusion. As the surface diffusion is enhanced if isolated adatoms can freely move along the surface without being hindered by other concurrently deposited adatoms, a

high degree of segregation is expected for low current densities (namely, due to the low deposition rate), whereas some intermixing of Co and Cu is expected for high current densities. On the other hand, the amount of Cu codeposited with Co increases with decreasing $j_{mag}$. This interplay of the codeposition and segregation of the species has the following effect on the microstructure and magnetic properties of ED Co-Cu/Cu multilayers.

At the highest current density ($j_{mag}$ = 84 mA/cm², sample A), the highly periodic multilayer grew with continuous Cu layers and with almost continuous Co layers. The total magnetoresistance of this multilayer was about 4.6 % (Fig. 1). The dominant part of MR (~93 %) came from the FM component, the complement from the SPM component. Cu layers were under tensile stress (Table 4), which was caused by the nature of the deposition process. The lattice misfit at the Co/Cu interfaces led to a higher tensile stress in Co layers in comparison with the Cu layers. However, the lattice strain in the Co layers was partly compensated by microstructure defects like microtwins and stacking faults that increased the interplanar spacing of Co in the direction of the multilayer growth [7]. A consequence of the interplay between the local lattice strains and the segregation of the species was a formation of highly correlated interface corrugations (Fig. 3) that grew throughout the whole multilayer stack.

At the medium current density ($j_{mag}$ = 20.7 mA/cm², sample B), Cu codeposited with Co segregated at the boundaries of the columnar grains (Fig. 4). The main consequences of the Cu segregation were a further increase of the amplitude of the interface corrugations and a large variation of the bilayer thickness as compared to sample A. Additionally, the Cu segregation increased the local strain fields in FM and NM layers (Table 4 and Fig. 10). The increase of the local strain fields and the observed compressive stress in Co layers can be explained by a lateral growth of Cu domains alongside the bits of the Co layers during the Cu segregation, which again contributed to the deepening of the interface corrugations. Nevertheless, the large but still highly correlated interface corrugations had no fatal consequences for the FM component of the magnetoresistance in sample B. Total MR increased to 5.2 % as driven by the increase of both FM and SPM components (Fig. 1). Still, the relative increase of the SPM component was larger than the increase of the FM component. The increase of the SPM component can be explained by fragmentation of magnetic layers as discussed in [11]. A possible reason for the increase of the FM component is the reduction of the density of point defects in FM layers due to the segregation of Cu from Co.

A further decrease of $j_{mag}$ to 9.6 mA/cm² (sample C) led to a high degree of Cu codeposition, which resulted in a considerable change of the overall chemical composition of the sample (Fig. 6), in the formation of Co precipitates embedded in Cu matrix (Fig. 2), in the decay of the FM component of MR and in the increase of the SPM contribution to the total

magnetoresistance (Fig. 1). Consequently, the total MR of 3.0 % arose mainly from the SPM component. The loss of a periodic multilayer structure led to a reduction of the lattice strains and to a leveling of the surface roughness. The formation of Co precipitates in Cu matrix is in fact an extrapolation of the multilayer model discussed for sample B to a much higher amount of Cu codeposited with Co. At the lowest current density $j_{mag}$, which was characterized by a preferential deposition of Cu and by a substantial segregation of species, the regions containing Cu were widely extended that led to the formation of separate Co seeds instead of forming continuous Co layers.

**5. Conclusions**

The results of this study have shown that the microstructure formation in Co-Cu/Cu multilayers deposited from a single bath is controlled by the competition between the codeposition of Cu with Co during the deposition of magnetic layers and the segregation of the species. High current density ($j_{mag}$ = 84 mA/cm²) facilitated growth of laterally continuous, periodic multilayers with large but highly correlated interface corrugations. A decrease of the current density to $j_{mag}$ = 20.7 mA/cm² led to the formation of columnar grains containing bits of the multilayer stack. The columnar grains were separated from each other by Cu domains. Other consequences of the segregation of the codeposited elements were a partial loss of the multilayer periodicity, an enhancement of the interface corrugations and an increase of the lattice strain in both non-magnetic and magnetic layers. A further reduction of the current density to $j_{mag}$ = 9.6 mA/cm² resulted in a preferential deposition of Cu at the expense of Co, which caused the formation of Co precipitates embedded in a Cu matrix. In general, decreasing $j_{mag}$ led to the loss of the lateral periodicity of the multilayers and to the fragmentation of magnetic layers, which enhanced the superparamagnetic contribution to the total magnetoresistance. Consequently, the ferromagnetic contribution to the total magnetoresistance declined with increasing discontinuity of the magnetic layers.

***Acknowledgements***

The financial support of the project # RA 1050/11-1 through the German Research Foundation (DFG) and the grant # NN 79846 through the Hungarian Scientific Research Fund (OTKA) are gratefully acknowledged. The TEM JEM 2010 FEF was purchased from the funds of the DFG priority program SPP 1062 and maintained from the funds of the project # RA 1050/R-12. Our special thanks go to Mrs. R. Popp for the TEM sample preparation.

***References:***


[1] G. Binasch, P. Grünberg, F. Saurenbach, W. Zinn, Phys. Rev. B 39 (1989) 4828.

[2] M.N. Baibich, J.M. Broto, A. Fert, F. Nguyen van Dau, F. Petroff, P. Etienne, G. Creuzet, A. Friedrich, J. Chazelas, Phys. Rev. Lett. 61 (1988) 2472.

[3] C.A. Ross, Ann. Rev. Mater. Sci. 24 (1994) 159.

[4] I. Bakonyi, L. Péter, Progr. Mater. Sci. 55 (2010) 107.

[5] L. Péter, A. Cziraki, L. Pogá, Z. Kupay, I. Bakonyi, M. Uhlemann, M. Herrich, B. Arnold, T. Bauer, K. Wetzig, J. Electrochem. Soc. 148 (3) (2001) C168-C176.

[6] A. Cziráki, L. Péter, B. Arnold, J. Thomas, H.D. Bauer, K. Wetzig, I. Bakonyi, Thin Solid Films 424 (2003) 229–238.

[7] D. Rafaja, C. Schimpf, V. Klemm, G. Schreiber, I. Bakonyi, L. Péter, Acta Mater. 57 (2009) 3211.

[8] V. Weihnacht, L. Péter, J. Tóth, J. Pádár, Z. Kerner, C.M. Schneider, I. Bakonyi, J. Electrochem. Soc. 150 (2003) C507.

[9] L. Péter, Q.X. Liu, Zs. Kerner, I. Bakonyi, Electrochim. Acta 49 (2004) 1513.

[10] E. Tóth-Kádár, L. Péter, T. Becsei, J. Tóth, L. Pogány, T. Tarnóczi, P. Kamasa, I. Bakonyi, G. Láng, Á. Cziráki, W. Schwarzacher, J. Electrochem. Soc. 147 (2000) 3311.

[11] Q.X. Liu, L. Péter, J. Pádár, I. Bakonyi, J. Electrochem. Soc. 152 (2005) C316.

[12] I. Bakonyi, L. Péter, Z. Rolik, K. Kiss-Szabó, Z. Kupay, J. Tóth, L.F. Kiss, J. Pádár, Phys. Rev. B 70 (2004) 054427.

[13] L. Péter, J. Pádár, E. Tóth-Kádár, Á. Cziráki, P. Sóki, L. Pogány, I. Bakonyi, Electrochim. Acta 52, 3813 (2007)

[14] A. Bartók, A. Csik, K. Vad, Gy. Molnár, E. Tóth-Kádár, L. Péter, J. Eletrochem. Soc. 156 (2009) D253.

[15] T. McGuire, R. Potter, IEEE Trans. Magn. 11 (1975) 1018.

[16] I. Bakonyi, E. Simon, B.G. Tóth, L. Péter, L.F. Kiss, Phys. Rev. B 79 (2009) 174421.

[17] E.E. Fullerton, I.K. Schuller, H. Vanderstraeten, Y. Bruynseraede, Phys. Rev. B 45 (1992) 9292.

[18] P. Nallet, E. Chassaing, M.G. Walls, M. Hÿtch, J. Appl. Phys. 79 (1996) 6884.

[19] D. Rafaja, H. Fuess, D. Šimek, L. Zdeborová, V. Valvoda, J. Phys.: Condens. Matter 14 (2002) 10021.

[20] L.G. Parratt, Phys. Rev. 95 (1954) 359.

[21] Y. Yoneda, Phys. Rev. 131 (1963) 2010.

[22] U. Pietsch, V. Holý, T. Baumbach, *High Resolution X-ray Scattering – From Thin Films to Lateral Nanostructures*, Springer, New York, 2004.

[23] S.K. Sinha, E.B. Sirota, S. Garoff, H.B. Stanley, Phys. Rev. B 38 (1988) 2297.

[24] V. Holý, J. Kuběna, I. Ohlídal, K. Lischka, W. Plotz, Phys. Rev. B 47 (1993) 15896.

[25] PDF-2 on CD-ROM. Newtown Square (PA): JCPDS-ICDD; 2003.

[26] A.J. Perry, V. Valvoda, D. Rafaja, Thin Solid Films 214 (1992) 169.

[27] M. Dopita, D. Rafaja, C. Wüstefeld, M. Růžička, V. Klemm, D. Heger, G. Schreiber, M. Šíma, Surf. Coat. Technol. 202 (2008) 3199.

[28] T.B. Massalski (Ed.), *Binary Alloy Phase Diagrams*, Second Edition plus Updates on CD-ROM, ASM International, Materials Park, Ohio, USA, 1996.

[29] P.E. Bradley, D. Landolt, Electrochim. Acta 45 (1999) 1077.

**Tables**

Table 1: Overview of deposition parameters (current density applied during the deposition of magnetic layers, $j_{mag}$, and the pulse duration, $\tau_{mag}$), the individual layer thicknesses t(Co-Cu) and t(Cu) determined from Faraday's law and the corresponding bilayer thickness $\Lambda$.

| Sample | $j_{mag}$ [mA/cm²] | $\tau_{mag}$ [s] | t(Co-Cu) [nm] | t(Cu) [nm] | $\Lambda$ [nm] |
|---|---|---|---|---|---|
| A | 84.0 | 0.12 | (3.3 ± 0.2) | (4.0 ± 0.2) | (7.3 ± 0.4) |
| B | 20.7 | 0.52 | (3.5 ± 0.2) | (4.2 ± 0.2) | (7.7 ± 0.4) |
| C | 9.6 | 1.00 | (3.1 ± 0.2) | (3.8 ± 0.2) | (6.9 ± 0.4) |

Table 2: Bilayer thickness ($\Lambda$), thicknesses of the individual layers [t(Co-Cu) and t(Cu)] and interplanar spacings in the sample surface perpendicular direction [d(Co-Cu) and d(Cu)] as obtained from the WAXS measurements.

| Sample | $\Lambda$ [nm] | t(Co-Cu) [nm] | t(Cu) [nm] | d(Co-Cu) [nm] | d(Cu) [nm] |
|---|---|---|---|---|---|
| A | (8.1 ± 0.1) | (3.68 ± 0.05) | (4.38 ± 0.05) | 0.2041(1) | 0.2083(1) |
| B | (7.8 ± 0.1) | (3.65 ± 0.05) | (4.15 ± 0.05) | 0.2051(1) | 0.2073(1) |

Table 3: Comparison of the structural characteristics of the ED Co-Cu/Cu multilayers obtained from Faraday's law and from the fitting of the WAXS patterns.

| Sample | $\Lambda_{WAXS}/\Lambda_F$ | $[t(Co\text{-}Cu)]_{WAXS}/[t(Co\text{-}Cu)]_F$ | $[t(Cu)]_{WAXS}/[t(Cu)]_F$ |
|---|---|---|---|
| A | (1.10 ± 0.05) | (1.11 ± 0.05) | (1.09 ± 0.05) |
| B | (1.01 ± 0.05) | (1.04 ± 0.05) | (0.99 ± 0.05) |

Table 4: Lattice strain obtained from the interplanar spacings measured in the sample surface perpendicular direction (Table 2) and related to $d^0_{111}$(Cu) = 0.20871 nm according to Eq. (4). The symbol $\langle\varepsilon_\perp$ (Co)$\rangle$ means the average of the lattice strains calculated for face centered cubic (fcc) and hexagonal close packed (hcp) cobalt.

| Sample | $\varepsilon_\perp$ (fcc-Cu) | $\varepsilon_\perp$ (fcc-Co) | $\varepsilon_\perp$ (hcp-Co) | $\langle\varepsilon_\perp$ (Co)$\rangle$ |
|---|---|---|---|---|
| A | $-1.88 \times 10^{-3}$ | $-2.60 \times 10^{-3}$ | $5.37 \times 10^{-3}$ | $1.38 \times 10^{-3}$ |
| B | $-6.72 \times 10^{-3}$ | $2.23 \times 10^{-3}$ | $10.24 \times 10^{-3}$ | $6.24 \times 10^{-3}$ |

Figure 1: (a) Magnetoresistance curves of the ED Co-Cu/Cu multilayers; solid and open symbols denote LMR and TMR, respectively. (b) Result of the decomposition of the longitudinal MR curves into the SPM (solid symbols) and FM (open symbols) components. (c) Magnified part of the MR curves from figure (a) showing the effect of the coercive field. Key to symbols: squares, circles and triangles refer to data for samples A, B and C, respectively.

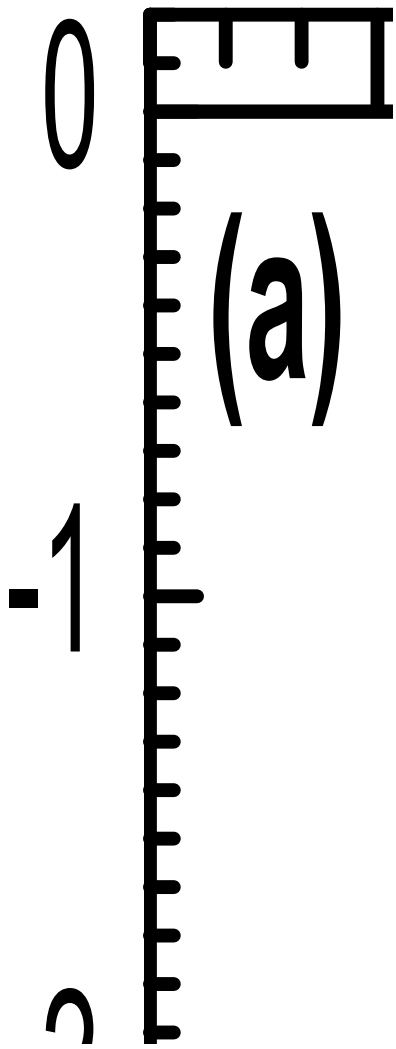


Figure 2: WAXS patterns of samples A, B and C taken in the vicinity of the diffraction lines 111 of fcc Cu and fcc Co. For samples A and B, the open symbols represent the measured data, the lines the fits according to [17]. For sample C, only the measured data (without the fit) are shown, because no superlattice satellites were observed.

Figure 3: TEM image of the multilayer stack from sample A taken in a strong overfocus showing almost continuous layers with highly correlated interface corrugations. The dashed line marks the direction parallel to the substrate surface, the dotted arrow the growth direction.

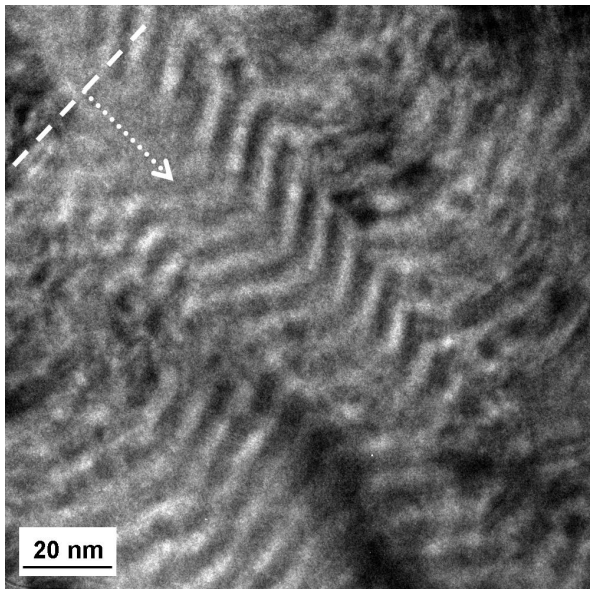


Figure 4: TEM image of the multilayer stack from sample B taken in diffraction contrast showing the formation of columnar grains that contain bits of the multilayer structure. The grain boundaries discussed in text are marked by solid arrows. The dashed line indicates the direction parallel to the substrate surface, the dotted arrow the growth direction.

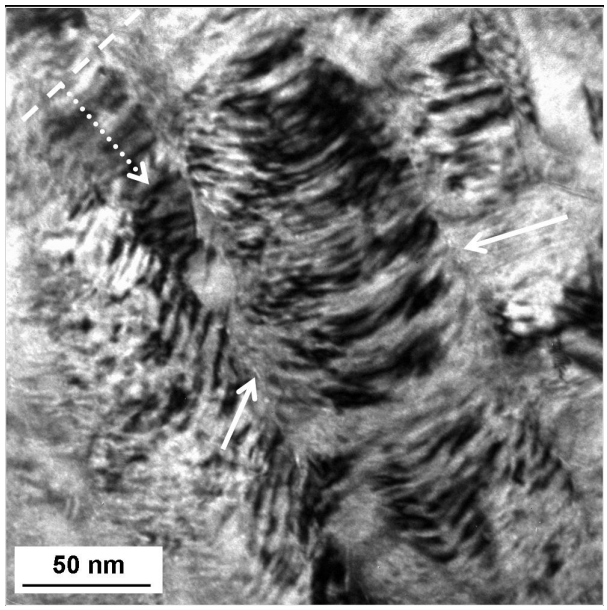


Figure 5: TEM image of sample C taken in diffraction contrast. No periodic multilayer structure was visible. The direction parallel to the substrate surface and the growth direction are marked by the dashed line and by the dotted arrow, respectively.

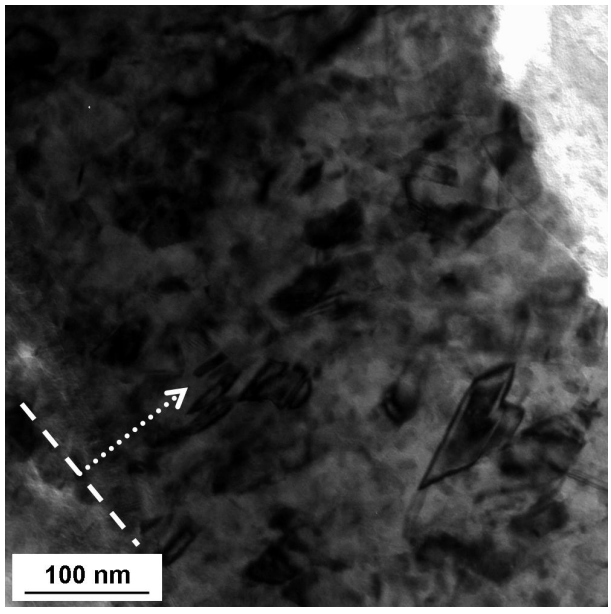

Figure 6: EDX spectra of samples A, B and C taken in TEM. The measured intensities were normalized on the intensity of the spectral line CuK$\alpha$ in order to illustrate the change in the Co/Cu ratio in sample C. During the measurement, the whole cross-section of the respective sample was irradiated by the electron beam.

Figure 7: Rocking curves of samples A, B and C taken in the SAXS mode. The detector angles were $2\theta$ = 1.33° for sample A, $2\theta$ = 1.48° for sample B and $2\theta$ = 1.49° for sample C. The angle $\omega$ means the inclination of the sample from the symmetrical position. The Yoneda wings observed in samples with a smaller surface roughness are labeled by arrows.

Figure 8: Surface morphology of the samples under study as seen by AFM.

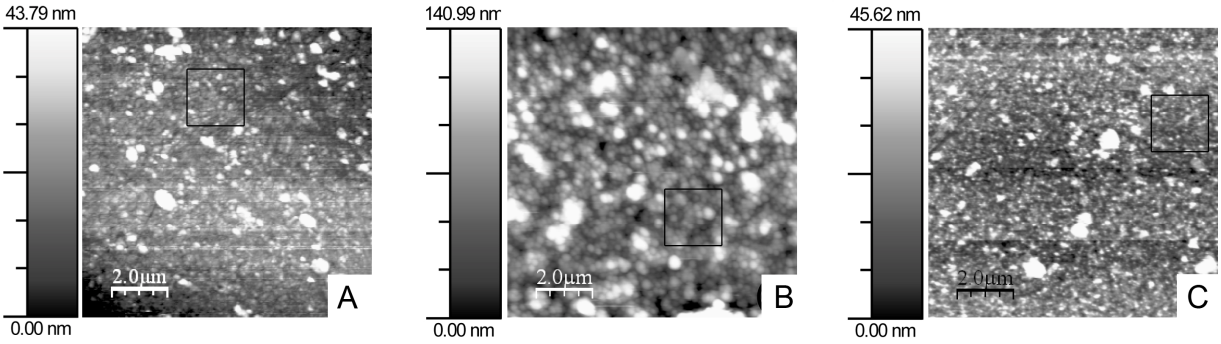


Figure 9: Microtwins within individual grains of sample B as seen by TEM in diffraction contrast. The microtwins are almost parallel to the surface of the substrate and almost perpendicular to the growth direction; the corresponding directions are marked by the dashed line and by the dotted arrow, respectively.

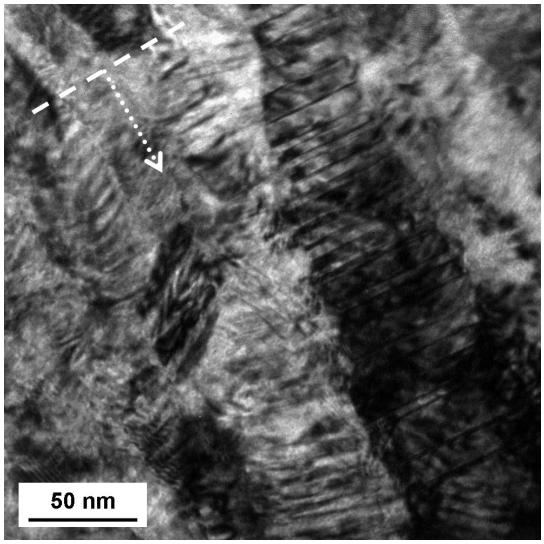


Figure 10: Coexistence of microtwins (grown perpendicular to the growth direction) and strain fields in Sample B. The latter were recognized by TEM carried out in diffraction contrast as dark arcs pinned at the grain boundaries. Some examples of the strain fields are labeled by solid arrows. The growth direction is marked by the dotted arrow.